



# Effects of Mn-Doping on the Structural and Electrochemical Properties of $\text{Na}_3\text{Ni}_2\text{SbO}_6$ for Sodium-Ion Battery

Yongho Kee,<sup>[a, b, c]</sup> Brecht Put,<sup>[b]</sup> Nikolay Dimov,<sup>[a]</sup> Aleksandar Staykov,<sup>[d]</sup> and Shigeto Okada<sup>\*[a]</sup>

Recently, layered O'3-Na<sub>3</sub>Ni<sub>2</sub>SbO<sub>6</sub> has been investigated as a unique cathode material for Na-ion batteries due to the good electrochemical performance via O'3-P'3 phase transitions in the voltage range between 2.0 and 4.0 V vs Na<sup>+</sup>/Na. However, at present it is not well understood whether transition metal doping of the pristine structure could improve the phase transition kinetics during charge/discharge. In this study, we synthesized Mn-doped Na<sub>3</sub>Ni<sub>2-x</sub>Mn<sub>x</sub>SbO<sub>6</sub> ( $x=0, 0.25, 0.5$ ) layered oxides and investigated their feasibility as cathode materials for

Na-ion batteries using ex-situ X-ray diffraction (XRD) coupled with DFT calculations. The results show that light Mn doping ( $x=0.25$ ) energetically enhances the O'3-P'3 phase transition kinetics with smaller unit-cell-volume changes. However, the heavily doped ( $x=0.5$ ) sample suffers from large polarization, which could be attributable to the reduced two-phase reaction range and a large unit-cell-volume change upon sodium extraction.

## 1. Introduction

Over the past few decades, lithium insertion materials for non-aqueous lithium-ion batteries have been widely investigated because of their long cycle life, low self-discharge rate, and high energy density compared to conventional aqueous batteries.<sup>[1-4]</sup> However, their high cost and the resource restrictions of lithium limit their further application in large-scale energy storage systems which are needed for grid level storage. This sparked a recent interest in the development of lower cost and more abundant chemistries, which could be either lithium-ion batteries without any costly metals such as cobalt, the main price-restrictive ingredient, or alternative chemistries. These should offer comparable electrochemical performance to that of lithium-ion batteries but with reduced dependence on both cobalt and lithium.

Since sodium is the most abundant alkali metal element in the earth's crust, sodium-ion batteries having working principles and performance similar to those of their lithium-ion counterparts could be regarded as a possible replacement for the current lithium-ion batteries.<sup>[5-7]</sup> So far, the designs for sodium-ion cathode host materials have been borrowed from

their well-known lithium equivalents. These include multi-dimensional structures with freely movable sodium ions such as Na<sub>x</sub>MO<sub>2</sub>,<sup>[8-12]</sup> Na<sub>x</sub>MAO<sub>4</sub>,<sup>[13-15]</sup> Na<sub>x</sub>MP<sub>2</sub>O<sub>7</sub>,<sup>[16-18]</sup> and Na<sub>x</sub>M<sub>2</sub>(PO<sub>4</sub>)<sub>3</sub>,<sup>[19]</sup> in which M is typically the transition metal. Nevertheless, most sodium-ion cathode materials show insufficient energy densities and poor cycle performances, further triggering the development of their cation-, anion-substituted derivatives or other more conductive carbon components.<sup>[20-22]</sup> Doping with either a transition or non-transition metal is a common practice in the design of intercalation hosts for lithium-ion and sodium-ion batteries. Doping with a suitable element is often an effective means to enhance the properties of the corresponding solid-state phases because of changes in the band gap (i.e., electrical conductivity) and the diffusion rate of Na<sup>+</sup>/Li<sup>+</sup> ions and/or the suppression of unwanted drastic phase transitions that induce a large unit cell volume expansion upon cation extraction.<sup>[23-27]</sup>

Recently, a layered sodium nickel antimony oxide, Na<sub>3</sub>Ni<sub>2</sub>SbO<sub>6</sub>, with the space group of C2/m (#12), which is also regarded as O'3-type Na[Ni<sub>2/3</sub>Sb<sub>1/3</sub>]O<sub>2</sub> according to Delmas' notation,<sup>[28,29]</sup> has been studied as a possible cathode for sodium-ion batteries. In that regard, Na<sub>3</sub>Ni<sub>2</sub>SbO<sub>6</sub> has shown decent electrochemical performance by virtue of the reversible insertion and extraction of two Na atoms per formula unit employing the Ni<sup>3+</sup>/Ni<sup>2+</sup> redox couple with the theoretical capacity of 132 mAh g<sup>-1</sup>.<sup>[30]</sup> On the other hand, there have hardly been any reports concerning the effects of doping with other metals for the Ni or Sb sites in the pristine structure and their corresponding electrochemical behavior, even though it is of both practical and theoretical interest to study whether Na<sub>3</sub>Ni<sub>2</sub>SbO<sub>6</sub> could form single phases of metal-doped derivatives while allowing reversible sodium insertion/extraction. Recently, Aguesse et al. reported a Zn-doped Na<sub>3</sub>Ni<sub>2</sub>SbO<sub>6</sub>,<sup>[31]</sup> and Zheng and coworkers also reported Na<sub>3</sub>Ni<sub>2</sub>BiO<sub>6</sub> for Na-ion batteries.<sup>[32]</sup> This latter material showed promising electrochemical activity as positive electrode materials in non-aqueous Na cells in which the extraction of the first two sodium atoms

[a] Dr. Y. Kee, Dr. N. Dimov, Prof. Dr. S. Okada  
Institute for Materials Chemistry and Engineering  
Kyushu University  
6-1, Kasuga-koen, Kasuga 816-8580 (Japan)  
E-mail: s-okada@cm.kyushu-u.ac.jp

[b] Dr. Y. Kee, Dr. B. Put

Estore  
imec  
Kapeldreef 75, 3001 Heverlee (Belgium)

[c] Dr. Y. Kee  
Centre of Surface Chemistry and Catalysis  
KU Leuven  
Kasteelpark Arenberg 23, 3001 Heverlee (Belgium)

[d] Prof. Dr. A. Staykov  
International Institute for Carbon-Neutral Energy Research (WPI-12CNER)  
Kyushu University  
744 Motoooka, Nishi-ku, Fukuoka 819-0395 (Japan)

per formula unit is associated with the phase transition from the O'3 to the P'3 phase. In fact, if the metal doping on this host could potentially decrease the cost of raw materials, it would stimulate the investigation of other compounds in the  $\text{Na}_3\text{M}_2\text{SbO}_6$  family and related O3/P2-type layered oxides.

Among various potential doping elements, Mn is one of the most preferable dopants as it is the third-most abundant transition metal element in the earth's crust and its oxide forms are usually stable in ambient air. Therefore, the partial replacement of Ni in  $\text{Na}_3\text{Ni}_2\text{SbO}_6$  with Mn may qualify its derivative as a promising cathode with a reduced raw materials cost. To check the feasibility of Mn-doped  $\text{Na}_3\text{Ni}_2\text{SbO}_6$  as a possible cathode material for Na-ion batteries, a series of  $\text{Na}_3\text{Ni}_{2-x}\text{Mn}_x\text{SbO}_6$  ( $x=0$ , 0.25, and 0.5) samples are synthesized and ex-situ X-ray diffraction (XRD) measurements are carried out to observe the structural variations of the Mn-doped title compounds during electrochemical sodium extraction. To further investigate the detailed phase transition kinetics of the title compounds, the unit cell volume and total energies of the initial and sodium-extracted phases are systematically calculated via DFT calculations. The doping amounts of  $x=1/8$  and  $1/4$  are selected, as those two derivatives showed quite different charge/discharge performances in our preliminary measurements. Performance was further studied, and the selected doping amounts could be manipulated using  $2 \times 1 \times 1$  supercells due to the small energy differences regardless of the selected Mn atoms in the supercell, which contains eight metal atoms. The primary goal of this study was to investigate the fundamental properties of the title compounds, such as the initial charge/discharge and the calculated band gap, and to provide a general understanding of O'3-P'3 phase transition kinetics for the title compounds using ex-situ XRD and DFT calculations.

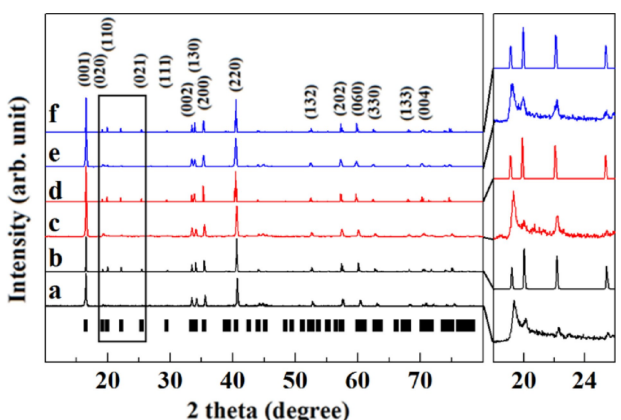


**Figure 1.** The obtained powder XRD patterns with their respective theoretically simulated powder XRD patterns of (a,b)  $\text{Na}_3\text{Ni}_2\text{SbO}_6$ , (c,d)  $\text{Na}_3\text{Ni}_{1.75}\text{Mn}_{0.25}\text{SbO}_6$ , and (e,f)  $\text{Na}_3\text{Ni}_{1.5}\text{Mn}_{0.5}\text{SbO}_6$ . Their corresponding low-angle reflections (squared) are magnified on the right side. The experimentally obtained reflections are further magnified for clarity.

## 2. Results and Discussion

Figure 1 shows the powder XRD patterns of  $\text{Na}_3\text{Ni}_2\text{SbO}_6$ ,  $\text{Na}_3\text{Ni}_{1.75}\text{Mn}_{0.25}\text{SbO}_6$ , and  $\text{Na}_3\text{Ni}_{1.5}\text{Mn}_{0.5}\text{SbO}_6$ , all whose diffraction peaks match well with those of previously reported  $\text{Na}_3\text{Co}_2\text{SbO}_6$  (ICSD #245538) with the space group of C2/m (#12). These data show that the target materials are synthesized as single phases without distinctive impurities via simple calcination. From the profile matching of XRD patterns for each compound, we estimated the unit cell volumes in a monoclinic system of  $260.12(2)$  Å<sup>3</sup>,  $264.22(3)$  Å<sup>3</sup>, and  $270.90(7)$  Å<sup>3</sup> for  $\text{Na}_3\text{Ni}_2\text{SbO}_6$ ,  $\text{Na}_3\text{Ni}_{1.75}\text{Mn}_{0.25}\text{SbO}_6$ , and  $\text{Na}_3\text{Ni}_{1.5}\text{Mn}_{0.5}\text{SbO}_6$ , respectively, which are in good agreement with the larger ionic radius of  $\text{Mn}^{2+}$  (0.83 Å) compared to that of  $\text{Ni}^{2+}$  (0.69 Å) in a six-coordination environment.<sup>[33]</sup> In our initial structure analysis using DFT calculations, we first simulated the initial honeycomb ordering with the space group of C2/m (#12) by assuming that the Mn atoms occupy the Sb sites sharing the same equivalent position, in order to check the possible disordering in the  $\text{Ni}_2\text{-Sb}$  honeycomb framework. However, this trial rapidly proved to be unphysical, likely due to the large difference in electronic density between Sb and Mn. To maintain the honeycomb ordering, only electronically heavy atoms such as Bi with similar physical properties could replace Sb.<sup>[34]</sup> Otherwise, the honeycomb ordering will be lost and the title compounds would stabilize as disordered phases, which are both structurally and electrochemically different from the honeycomb-ordered structure.<sup>[35]</sup> Therefore, we assumed that in this study the Mn atoms were introduced into the Ni sites maintaining the same space group of C2/m (#12) without the destruction of the honeycomb ordering. This assumption was reasonable for the theoretically simulated initial models shown in Figure 1, with similar unit cell volumes of  $263.13$  Å<sup>3</sup>,  $266.39$  Å<sup>3</sup>, and  $265.27$  Å<sup>3</sup> for  $\text{Na}_3\text{Ni}_2\text{SbO}_6$ ,  $\text{Na}_3\text{Ni}_{1.75}\text{Mn}_{0.25}\text{SbO}_6$ , and  $\text{Na}_3\text{Ni}_{1.5}\text{Mn}_{0.5}\text{SbO}_6$ , respectively.

In fact, the valence and non-stoichiometry of the nickel, manganese, and antimony in the products have not been experimentally clarified in this study. However, our bond-valence-sum calculations using the theoretically simulated structures revealed that the valence of Ni is predicted to be +1.738 for pristine  $\text{Na}_3\text{Ni}_2\text{SbO}_6$ , while slightly higher valence values of +1.972 and +2.209 were predicted for Mn in  $\text{Na}_3\text{Ni}_{1.75}\text{Mn}_{0.25}\text{SbO}_6$  and  $\text{Na}_3\text{Ni}_{1.5}\text{Mn}_{0.5}\text{SbO}_6$ , respectively. This is to say, light doping ( $x \sim 0.25$ ) increases the average valence of the metal sites by 0.029 and heavy doping ( $x \sim 0.5$ ) increases the average valence of the metal sites by 0.118. Since these calculations are based on the ground state, these effects could be slightly underestimated.<sup>[36,37]</sup> From a profile-matching series for the prepared samples, we obtained a Bragg R-factor ( $R_B$ ) of 3.62% for pristine  $\text{Na}_3\text{Ni}_2\text{SbO}_6$ , which was similar to that (2.22%) of  $\text{Na}_3\text{Ni}_{1.75}\text{Mn}_{0.25}\text{SbO}_6$ , while a slightly higher  $R_B$  factor of 6.80% was observed from  $\text{Na}_3\text{Ni}_{1.5}\text{Mn}_{0.5}\text{SbO}_6$ . The reason for this subtle difference is not clear. However, material optimization using a systematic methodology such as factorial experiments needs to be applied to find the ideal synthetic conditions for a more reliable refinement of the crystal structure of the  $\text{Na}_3\text{M}_2\text{SbO}_6$  family in the future. On the other

hand, our preliminary computational investigation revealed that Mn doping leads to a narrower band gap with slightly reduced electronic energy density near the Fermi level, as illustrated in Figure 2. Although the calculated density of state (DOS) is often overestimated,<sup>[38]</sup> the reduced band gaps for the Mn-doped  $\text{Na}_3\text{Ni}_2\text{SbO}_6$  are in good agreement with the darker color of the Mn-doped  $\text{Na}_3\text{Ni}_2\text{SbO}_6$  powders.

To evaluate the feasibility of the title compounds as cathode materials for Na-ion batteries, their electrode properties were examined in non-aqueous Na cells in the voltage range between 2.0 and 4.0 V at room temperature, as illustrated in Figure 3. Similar initial sodiation capacities of  $98 \text{ mAh g}^{-1}$  for  $\text{Na}_3\text{Ni}_2\text{SbO}_6$  and  $93 \text{ mAh g}^{-1}$  for  $\text{Na}_3\text{Ni}_{1.75}\text{Mn}_{0.25}\text{SbO}_6$  were observed, respectively, with an average redox potential of ca. 3.3 V and 85% and 89% capacity retention rates for  $\text{Na}_3\text{Ni}_2\text{SbO}_6$  and  $\text{Na}_3\text{Ni}_{1.75}\text{Mn}_{0.25}\text{SbO}_6$  after 35 cycles, respectively. Here, the obtained irreversible capacities in their initial cycles show that the initial O'3 phase may undergo irreversible phase transition to minor phases after their first phase transition to P'3 phase.<sup>[30]</sup> When we tested the rate capability, the decrease in the specific capacity at higher

current rates ( $> 1 \text{ C}$ ) was clearly mitigated by light manganese doping. From Figure 3, specific capacities of  $51 \text{ mAh g}^{-1}$  and  $64 \text{ mAh g}^{-1}$  for  $\text{Na}_3\text{Ni}_2\text{SbO}_6$  and  $\text{Na}_3\text{Ni}_{1.75}\text{Mn}_{0.25}\text{SbO}_6$  were observed, respectively, at a current rate of 2 C. On the other hand, a considerable decrease in the initial capacity of  $34 \text{ mAh g}^{-1}$  was observed due to the huge polarization for  $\text{Na}_3\text{Ni}_{1.5}\text{Mn}_{0.5}\text{SbO}_6$ , as seen in Figure 3.

To better understand the rate dependence of the title compounds, the kinetics of sodium extraction and insertion should correlate with the reversible phase transitions between O'3 and P'3 for  $\text{Na}_y\text{Ni}_2\text{SbO}_6$  ( $y=3$  to 1), as reported previously.<sup>[30]</sup> Figure 4a illustrates the schematic views of the O'3- $\text{Na}_3\text{Ni}_2\text{SbO}_6$  and P'3- $\text{Na}_3\text{Ni}_2\text{SbO}_6$  crystal structures.<sup>[30,31]</sup> The phase transition between O'3 and P'3 is known to reversibly proceed through the  $\text{MO}_2$  slab gliding mechanism without breaking the M–O bond. As a result, both the O'3 and P'3 phases share the same honeycomb ordering of Ni and Sb cations in the transition metal layer. However, slight distortion due to the Na redistribution classifies the O'3 phase as physically unidentical from the P'3 phase.<sup>[39]</sup>

To further investigate the effects of the structural modification of the title compounds upon Na extraction, ex-situ XRD of the charged and discharged composite electrodes are also shown in Figure 4. By disassembling the Na cells initially charged up to 4.0 V, we prepared three different desodiated electrodes with net formulas of  $\text{Na}_y\text{Ni}_2\text{SbO}_6$ ,  $\text{Na}_y\text{Ni}_{1.75}\text{Mn}_{0.25}\text{SbO}_6$ , and  $\text{Na}_y\text{Ni}_{1.5}\text{Mn}_{0.5}\text{SbO}_6$  ( $y$ =the amount of sodium left after desodiation) for the ex-situ XRD measurement. In the diffraction patterns, the reflections of the desodiated P'3-type phase became predominant for  $\text{Na}_y\text{Ni}_2\text{SbO}_6$  and  $\text{Na}_y\text{Ni}_{1.5}\text{Mn}_{0.5}\text{SbO}_6$ , while the weak and broadened reflections of the O'3 and P'3 phases were observed for  $\text{Na}_y\text{Ni}_{1.75}\text{Mn}_{0.25}\text{SbO}_6$ . Here, the extraction of more than two sodium ions per initial formula unit for  $\text{Na}_3\text{Ni}_2\text{SbO}_6$  and  $\text{Na}_3\text{Ni}_{1.75}\text{Mn}_{0.25}\text{SbO}_6$  could be attributable to the possible phase transition from the P'3 to the O1 phase or to minor side reactions<sup>[30]</sup> which are represented as steep charging curves starting from 3.5 V vs  $\text{Na}^+/\text{Na}$  with a relatively small reversible capacity ( $\sim 0.05 \text{ Na}$ ) in the following cycles. However, since the possible phase transition from P'3 to O1 has not contributed directly to the charge and discharge curves in the second cycles and the generation of any distinguishable reflection for the O1 phase in our ex-situ diffraction measurements, it is reasonable to assume that the majority of initially charged samples have the empirical formulae of  $\text{Na}_3\text{Ni}_2\text{SbO}_6$  and  $\text{Na}_3\text{Ni}_{1.75}\text{Mn}_{0.25}\text{SbO}_6$ , respectively, explaining the relatively high initial charging capacity. On the other hand, the extraction of two sodium ions from initial  $\text{Na}_3\text{Ni}_{1.5}\text{Mn}_{0.5}\text{SbO}_6$  could not be completed. To fully understand the possible sodium extraction mechanism between  $\text{NaM}_2\text{SbO}_6$  and  $\text{M}_2\text{SbO}_6$ , the structural stability and reversibility for both the P'3 and O1 phases should be further investigated. We also measured the ex-situ diffraction of each sample after discharging process. It was found that the P'3 phase reverted back to its initial form (O'3 phase) for  $\text{Na}_y\text{Ni}_{1.75}\text{Mn}_{0.25}\text{SbO}_6$ , while only a portion of the P'3 phase reverted back to the O'3 phase for  $\text{Na}_y\text{Ni}_2\text{SbO}_6$ . However, the P'3 phase remained almost intact for  $\text{Na}_y\text{Ni}_{1.5}\text{Mn}_{0.5}\text{SbO}_6$ , which should be attributable to the irreversible capacity observed in Figure 3. This observation is in good agreement with previously reported Mg-doped  $\text{Na}_3\text{Ni}_2\text{SbO}_6$ , where a smooth phase transition between the

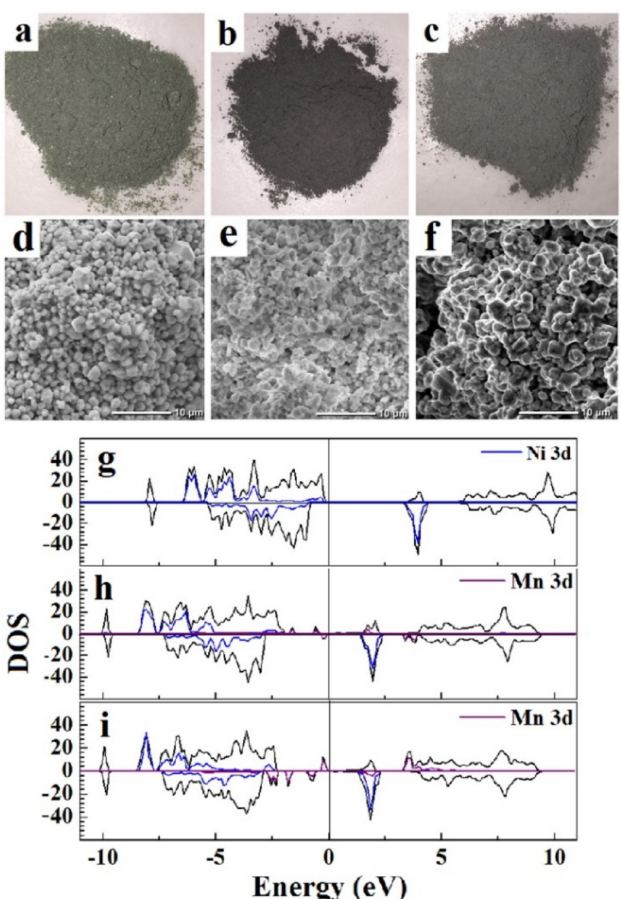


**Figure 2.** Photos showing the color of (a)  $\text{Na}_3\text{Ni}_2\text{SbO}_6$ , (b)  $\text{Na}_3\text{Ni}_{1.75}\text{Mn}_{0.25}\text{SbO}_6$ , and (c)  $\text{Na}_3\text{Ni}_{1.5}\text{Mn}_{0.5}\text{SbO}_6$  powders, and their corresponding SEM images for (d)  $\text{Na}_3\text{Ni}_2\text{SbO}_6$ , (e)  $\text{Na}_3\text{Ni}_{1.75}\text{Mn}_{0.25}\text{SbO}_6$ , and (f)  $\text{Na}_3\text{Ni}_{1.5}\text{Mn}_{0.5}\text{SbO}_6$ . The calculated total densities of state (DOS) profiles (black), partial densities of state profiles of Ni (blue) and Mn (purple) for (g)  $\text{Na}_3\text{Ni}_2\text{SbO}_6$ , (h)  $\text{Na}_3\text{Ni}_{1.75}\text{Mn}_{0.25}\text{SbO}_6$ , and (i)  $\text{Na}_3\text{Ni}_{1.5}\text{Mn}_{0.5}\text{SbO}_6$  are also shown.

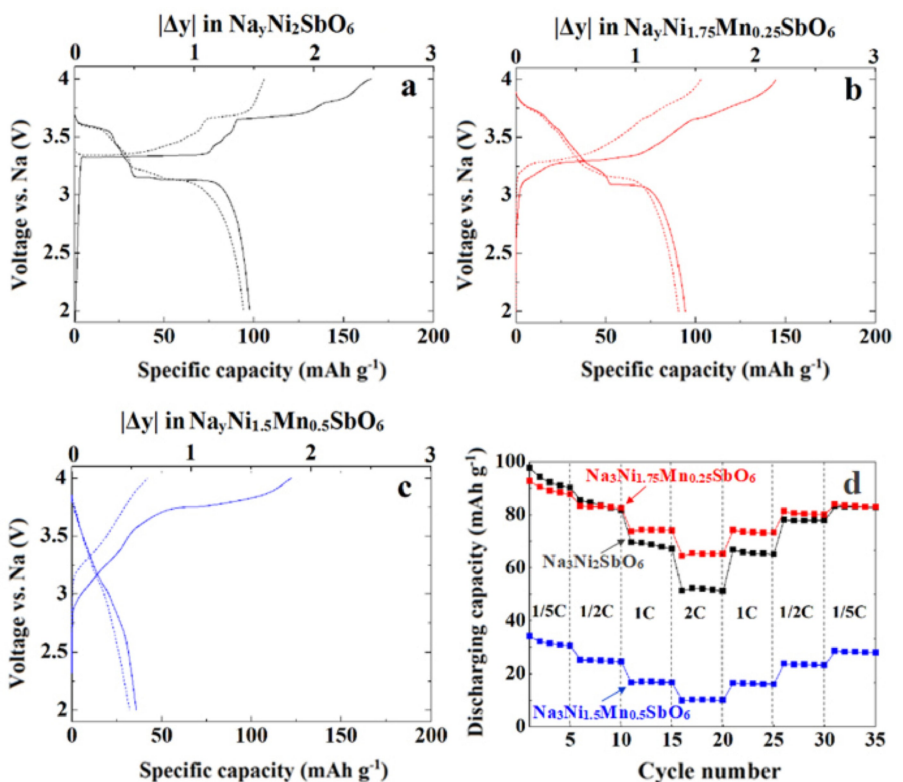


**Figure 3.** First (solid) and second (dashed) charge and discharge curves of (a)  $\text{Na}_3\text{Ni}_2\text{SbO}_6$ , (b)  $\text{Na}_3\text{Ni}_{1.75}\text{Mn}_{0.25}\text{SbO}_6$ , (c)  $\text{Na}_3\text{Ni}_{1.5}\text{Mn}_{0.5}\text{SbO}_6$ , and their rate-dependent discharge capacities (d).

initial O'3 and desodiated P'3 phases resulted in improved rate performance.<sup>[40]</sup> On the other hand, the broadened reflections observed in this study might be attributable to a number of stacking-fault phases which have been reported before in similar materials.<sup>[41,42]</sup> Although the exact mass ratios of O'3, P'3, and other minor phases such as the O1 phase for each compound at the end of charge and discharge are not clearly identified, the results from a series of profile matches for the charged samples, using the most distinctive reflections obtained from ex-situ XRD measurements, match well with the theoretically calculated structures within a small range of experimental error (~2%). For example, the experimentally obtained unit cell volumes using the most distinctive reflections for charged P'3 phases with the net formulae of  $\text{Na}_3\text{Ni}_2\text{SbO}_6$ ,  $\text{Na}_y\text{Ni}_{1.75}\text{Mn}_{0.25}\text{SbO}_6$ , and  $\text{Na}_y\text{Ni}_{1.5}\text{Mn}_{0.5}\text{SbO}_6$  were estimated to be  $269.4 \text{ \AA}^3$ ,  $269.4 \text{ \AA}^3$ , and  $272.4 \text{ \AA}^3$ , respectively, while the theoretically calculated unit cell volumes for P'3- $\text{NaNi}_2\text{SbO}_6$ , P'3- $\text{NaNi}_{1.75}\text{Mn}_{0.25}\text{SbO}_6$ , and P'3- $\text{NaNi}_{1.5}\text{Mn}_{0.5}\text{SbO}_6$  were  $273.2 \text{ \AA}^3$ ,  $274.4 \text{ \AA}^3$ , and  $275.1 \text{ \AA}^3$ , respectively. This result shows that the majority of the charged samples exist as P'3- $\text{Na}_y\text{M}_2\text{SbO}_6$ , where  $y$  is close to 1 after the initial sodium extraction. Nevertheless, further characterization should be carried out to fully understand the detailed phase transition kinetics between the O'3 and P'3 phases.

In such cases, DFT calculations could provide insights into atomic scale information for a system in which the movement of a single atom and electron could be artificially manipulated and recorded to predict possible structural variations and potential influences on corresponding electronic structures. Our preliminary

searches for possible inequivalence among independent atomic positions automatically generated from  $P1$  symmetry resulted in negligible differences in the range of standard convergence criteria of the electronic relaxation cycle ( $10^{-5} \text{ eV/atom}$ ); therefore, the net formation energies and changes in unit cell parameters calculated in this study are assumed to be comparable to each other due to the crystallographically equivalent positions of Ni and Na in the  $C2/m$  symmetry of  $\text{Na}_3\text{Ni}_2\text{SbO}_6$ . The formation energy ( $E_f$ ) of an intermediate phase  $\text{Na}_y\text{Ni}_2\text{SbO}_6$  with respect to the phase separation to the portion of the two end members, O'3- $\text{Na}_a\text{Ni}_2\text{SbO}_6$  and P'3- $\text{Na}_b\text{Ni}_2\text{SbO}_6$ , could be described as follows:<sup>[43]</sup>

$$E_f = E(\text{Na}_y\text{Ni}_2\text{SbO}_6) - zE(\text{O}'3-\text{Na}_a\text{Ni}_2\text{SbO}_6) - (1-z)E(\text{P}'3-\text{Na}_b\text{Ni}_2\text{SbO}_6),$$

where  $E(\text{Na}_y\text{Ni}_2\text{SbO}_6)$  is the total energy of an intermediate  $\text{Na}_y\text{Ni}_2\text{SbO}_6$ ,  $E(\text{O}'3-\text{Na}_a\text{Ni}_2\text{SbO}_6)$  is the total energy of the initial O'3- $\text{Na}_a\text{Ni}_2\text{SbO}_6$ ,  $E(\text{P}'3-\text{Na}_b\text{Ni}_2\text{SbO}_6)$  is the total energy of desodiated P'3- $\text{Na}_b\text{Ni}_2\text{SbO}_6$ ,  $z$  is the ratio of each component, and  $a$  and  $b$  are sodium mole fractions for the end members used in the calculation.

Figure 5 shows the formation energies of all intermediate phases having different sodium contents. Here, the positive formation energy means that the starting O'3-type phase is stable without phase separation and the transition to the P'3 phase occurs when Na contents are forced to change by electrochemical means.<sup>[44]</sup> In other words, the phase transition from O'3 to P'3 occurs when the calculated formation energy

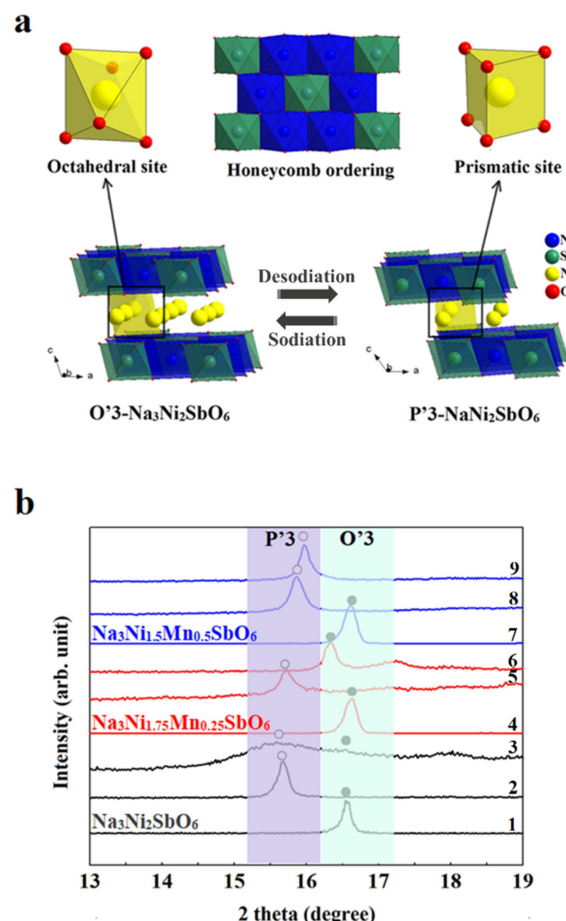


**Figure 4.** Schematic views of pristine O'3-Na<sub>3</sub>Ni<sub>2</sub>SbO<sub>6</sub>, desodiated P'3-Na<sub>3</sub>Ni<sub>2</sub>SbO<sub>6</sub> phases along the *b*-axis (a), and low-angle ex-situ XRD patterns (b) of (1) Na<sub>3</sub>Ni<sub>2</sub>SbO<sub>6</sub> after (2) charging and (3) discharging, (4) Na<sub>y</sub>Ni<sub>1.75</sub>Mn<sub>0.25</sub>SbO<sub>6</sub> after charging (5) and discharging (6); and (7) Na<sub>y</sub>Ni<sub>1.75</sub>Mn<sub>0.25</sub>SbO<sub>6</sub> after charging (8) and discharging (9). Black and empty circles are indicative of the most distinctive peaks of the O'3 and P'3 phases, respectively.

becomes negative to adapt the lower contents of Na with energetically favorable arrangements. The figure shows that, by the desodiation of one sodium ion per formula,  $y=3$  to 2, the O'3 phase is energetically favorable for the title compounds with minimum changes in unit cell volume. However, when more sodium ( $y<1.5$  Na) is deintercalated from the framework, the formation energies of the pristine structures become much smaller,  $-0.68$  meV/atom and  $0.98$  meV/atom, for Na<sub>1.5</sub>Ni<sub>2</sub>SbO<sub>6</sub> and Na<sub>1.5</sub>Ni<sub>1.75</sub>Mn<sub>0.25</sub>SbO<sub>6</sub>, respectively, approaching 0 eV. This indicates that they possibly coexist as two phases, a sodium-rich O'3 phase and a sodium-poor P'3 phase, while the formation energy of Na<sub>y</sub>Ni<sub>1.5</sub>Mn<sub>0.5</sub>SbO<sub>6</sub> clearly became negative in the range between  $y=2.0$  and  $1.5$ . This result indicates that the heavy Mn doping ( $x=0.5$ ) reduces the two-phase reaction range, while the light Mn doping ( $x=0.25$ ) increases the two-phase reaction range for Na<sub>3</sub>Ni<sub>2</sub>SbO<sub>6</sub>. These results agree well with the obtained galvanostatic charge/discharge profiles and ex-situ XRD data as described in Figure 3 and Figure 4, respectively.

The unit cell parameters and the volume changes in the optimized cells with the energetically most favorable routes for

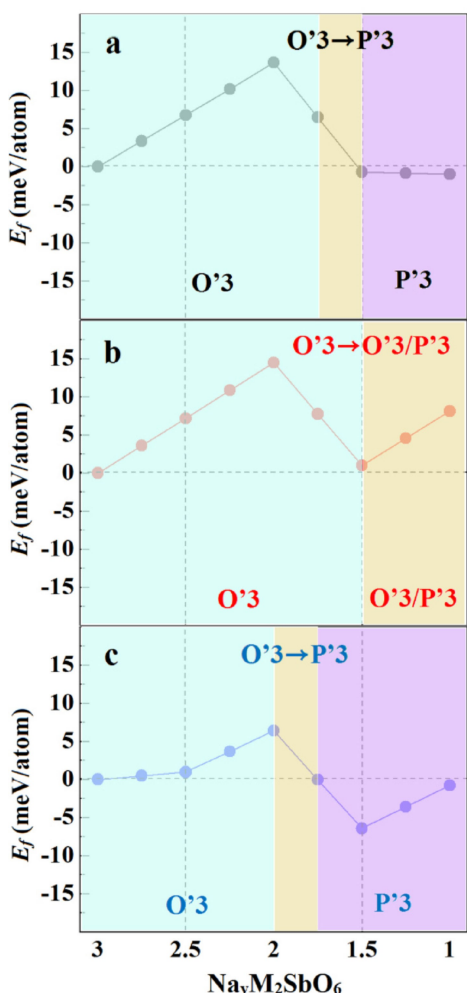


**Figure 5.** The formation energy ( $E_f$ ) of (a) Na<sub>y</sub>Ni<sub>2</sub>SbO<sub>6</sub>, (b) Na<sub>y</sub>Ni<sub>1.75</sub>Mn<sub>0.25</sub>SbO<sub>6</sub>, and (c) Na<sub>y</sub>Ni<sub>1.5</sub>Mn<sub>0.5</sub>SbO<sub>6</sub> with respect to phase separation and transition to P'3 phases.

the O'3 and P'3 phase transitions are simulated by DFT calculations as shown in Figure 6. The smallest change in unit cell volume of +1.0% was obtained for Na<sub>y</sub>Ni<sub>1.75</sub>Mn<sub>0.25</sub>SbO<sub>6</sub>, while much higher changes, of +4.0% for Na<sub>y</sub>Ni<sub>2</sub>SbO<sub>6</sub> and +10.3% for Na<sub>y</sub>Ni<sub>1.5</sub>Mn<sub>0.5</sub>SbO<sub>6</sub>, were obtained from the calculation. The difference in the subsequent unit cell volume change was predicted to be large between P'3-Na<sub>y</sub>Ni<sub>2</sub>SbO<sub>6</sub> (+0.1%) and P'3-Na<sub>y</sub>Ni<sub>1.5</sub>Mn<sub>0.5</sub>SbO<sub>6</sub> (-2.2%). Meanwhile, the subsequent unit cell volume change for P'3-Na<sub>y</sub>Ni<sub>1.75</sub>Mn<sub>0.25</sub>SbO<sub>6</sub> was calculated to be +1.7%. In addition, it is widely known that phases with smaller unit cell volume changes upon sodium extraction show greater electrochemical performance at high current rates than those with considerable changes in unit cell volume.<sup>[40,45,46]</sup> This further explains the greater rate capability of the lightly doped sample compared to the other two samples examined in this study.

Subsequently, a series of calculations showed that Na<sub>y</sub>Ni<sub>1.5</sub>Mn<sub>0.5</sub>SbO<sub>6</sub> undergoes the largest unit cell volume changes during both the O'3→P'3 phase transition and the subsequent sodium extraction reaction P'3→P'3, while Na<sub>y</sub>Ni<sub>2</sub>SbO<sub>6</sub> undergoes a major unit cell volume change when the O'3→P'3 phase transition occurs and Na<sub>y</sub>Ni<sub>1.75</sub>Mn<sub>0.25</sub>SbO<sub>6</sub>

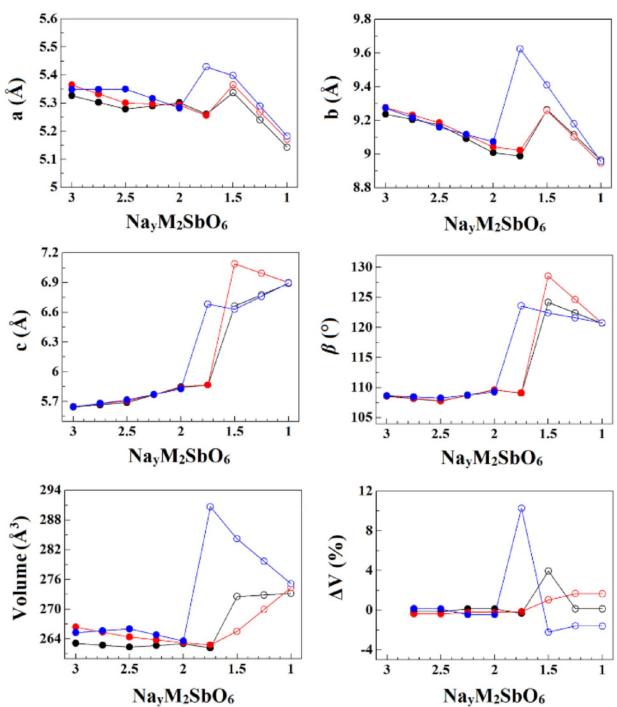


**Figure 6.** The calculated unit cell parameters and unit cell volume changes for the O'3 phase (filled circle) and the P'3 phase (empty circle) for  $\text{Na}_3\text{Ni}_2\text{SbO}_6$  (black),  $\text{Na}_3\text{Ni}_{1.75}\text{Mn}_{0.25}\text{SbO}_6$  (red), and  $\text{Na}_3\text{Ni}_{1.5}\text{Mn}_{0.5}\text{SbO}_6$  (blue). These results are based on the most energetically favorable routes of phase transition from the O'3 to the P'3 phase for each sample.

undergoes a major unit cell volume change during the  $\text{P}'3 \rightarrow \text{P}'3$  sodium extraction reaction, in which no phase transition occurs. These results are in good agreement with the partial reversibility of  $\text{P}'3\text{-Na}_3\text{Ni}_2\text{SbO}_6$  and the incomplete reversibility of  $\text{P}'3\text{-Na}_y\text{Ni}_{1.5}\text{Mn}_{0.5}\text{SbO}_6$  to O'3 phases upon recharge. On the other hand, the reversibility of the phase transition between O'3- and  $\text{P}'3\text{-Na}_y\text{Ni}_{1.75}\text{Mn}_{0.25}\text{SbO}_6$  upon sodium reinsertion becomes energetically preferred as well as kinetically faster, which is due to the smaller unit cell volume change for the  $\text{O}'3 \rightarrow \text{P}'3$  phase transition through the investigated range,  $y=3$  to 1, having positive formation energies with regard to both phases, O'3 and P'3. This result would also explain well the partial phase transition to the P'3 phase with the broadened reflections for  $\text{Na}_y\text{Ni}_{1.75}\text{Mn}_{0.25}\text{SbO}_6$  upon desodiation.

The results obtained from the DFT calculations are summarized as follows: (i) light Mn doping ( $x=0.25$ ) allows the energetically smooth O'3-P'3 phase transition upon recharge owing to the reduced unit cell volume changes upon recharge; and (ii) heavy Mn doping ( $x=0.5$ ) brings about the enhanced unit cell volume changes associated with huge polarization upon recharge due to the energetically reduced two-phase reaction range. We believe that the partial substitution of metal cations for transition metals in layered sodium transition metal oxides should be investigated by a proper combination of experimental and computational approaches to determine an efficient doping protocol and optimal composition for the realization of advanced sodium-ion battery performance.

### 3. Conclusions

The pristine sodium nickel antimony oxide and its Mn-doped derivatives with the empirical formula of  $\text{Na}_3\text{Ni}_{2-x}\text{Mn}_x\text{SbO}_6$  ( $x=0, 0.25$ , and  $0.5$ ) were synthesized and examined as cathode materials for Na-ion batteries in the voltage range between 2.0 and 4.0 V. To investigate the structural behaviors of each sample upon sodium extraction and insertion, the X-ray diffraction patterns of each sample after initial charge and discharge were recorded ex-situ and their detailed structural modifications were calculated using DFT calculations. Although they have the same honeycomb-type O'3 framework, the title compounds showed different specific capacities and rate capabilities. Our computational results revealed that light Mn doping ( $x=0.25$ ) on  $\text{Na}_3\text{Ni}_{2-x}\text{Mn}_x\text{SbO}_6$  resulted in smoother O'3-P'3 phase transition kinetics with smaller changes in the unit cell volume, whereas the completely opposite trend was observed when heavy Mn doping ( $x=0.5$ ) was applied. Since this is the first report on Mn doping on  $\text{Na}_3\text{Ni}_2\text{SbO}_6$  to show obvious differences in electrochemical properties depending on doping amounts, we suggest that other compounds in the  $\text{Na}_3\text{Ni}_{2-x}\text{M}_x\text{SbO}_6$  family ( $M=\text{transition metal}$ ) could qualify as possible cathode materials for Na-ion batteries.

### Experimental Section

Stoichiometric mixtures of the starting materials,  $\text{Na}_2\text{CO}_3$  (Wako),  $\text{Sb}_2\text{O}_3$  (Sigma-Aldrich),  $\text{NiO}$  (Sigma-Aldrich), and  $\text{MnO}$  (Sigma-Aldrich), were ball-milled in a planetary mill at 300 rpm for 1 h. The ball-to-powder ratio was 10:1 in mass. The precursor mixtures were poured into alumina crucibles and were gradually heated in a tube furnace up to 900 °C at a heating rate of 180 °C h<sup>-1</sup>. The temperature was then kept at 900 °C for 10 h under a steady Ar flow. These precursor mixtures were then cooled to room temperature at a cooling rate of 90 °C h<sup>-1</sup>. The resulting products were ground and heated again under a steady Ar flow before characterization using a Rigaku X-ray diffractometer (Cu-Kα, 50 kV, 300 mA). The preliminary unit cell parameter indexing, and profile matching of each sample were carried out by the Fullprof Suite refinement program, and the results were compared with the previously reported  $\text{Na}_3\text{Co}_2\text{SbO}_6$  (ICSD #245538). The background of the XRD profile was fitted with linear interpolation between a set of 59 points with refinable heights. The peak shape was refined by the convolution of a pseudo-Voigt function without refining the atomic positions and isotropic displacement parameters of each site. The unit cell parameters were then simulated using DFT calculations before bond-valence-sum calculations were further performed on the doubled unit cell for each sample to envisage the theoretical valence of each element.

For electrochemical tests in Na cells, composite electrodes were prepared by ball-milling a mixture of active material of the synthesized oxides and acetylene black (AB) (70:25 m/m) for 1 h at 300 rpm. The obtained active material/AB mixtures were blended with 5 wt% of PVDF binder, and the resulting electrode slurries in NMP solvent were pasted on Al-foils with a doctor blade. R2032 coin-type Na cells were assembled in an Ar-filled glove box and examined versus Na-metal using 1 M  $\text{NaPF}_6$ /PC:FEC (97:3 in vol%) electrolyte in the voltage range between 2.0 and 4.0 V vs  $\text{Na}^+/\text{Na}$  at room temperature around 25 °C. The ex-situ XRD profiles of the tested electrodes were measured by disassembling the tested Na cells after initial charging and discharging in the 20 range of 10–80° at a scan rate of 2° min<sup>-1</sup> with a step size of 0.02°.

The computational simulations were carried out using the periodic plane-wave density functional theory as implemented in the Vienna Ab initio Simulation Package (VASP) within the projector augmented-wave approach using the Perdew-Burke-Ernzerhof generalized-gradient approximation (GGA) function.<sup>[47,48]</sup> Projector-augmented wave (PAW) pseudopotentials with an electron cutoff energy of 520 eV and (4×4×6) Monkhorst-Pack k-point sampling grids were set to obtain the energy and the relaxed geometry of 2×1×1 Na<sub>y</sub>M<sub>2</sub>SbO<sub>6</sub> ( $y=3.0, 2.5, 2.0, 1.5, 1.0$ ) supercells. In fact, the introduction of more than two Mn atoms in a single unit cell to treat other doping amounts, such as  $x=3/8$ , results in a combination of various structures with different unit cell volumes and total energies depending on the selection of the metal site for the substitution and the remaining sodium atoms for other stoichiometric intermediate forms. Here, we focus exclusively on two structures with doping amounts of  $x=1/8$  and 1/4 to prevent the calculated data from being misleading. Unit cells with variable Na content were necessary to calculate the unit cell volume and energy variations at different Mn-doping levels during sodium extraction. Since the reversible insertion/extraction of more than two Na per formula unit with additional phase transformations to other minor phases was estimated to be negligible, in this study we focus on possible structural reversibility between two main phases ( $y=3-1$  in Na<sub>y</sub>M<sub>2</sub>SbO<sub>6</sub>), i.e., the initial O'3-type phase and the desodiated P'3-type phase.

## Conflict of Interest

The authors declare no conflict of interest.

**Keywords:** doping • layered oxides • Na<sub>3</sub>Ni<sub>2</sub>SbO<sub>6</sub> • phase transitions • sodium-ion batteries

- [1] K. Mizushima, P. C. Jones, P. J. Wiseman, J. B. Goodenough, *Mater. Res. Bull.* **1980**, *15*, 783–789.
- [2] T. Nohma, H. Kurokawa, M. Uehara, M. Takahashi, K. Nishio, T. Saito, *J. Power Sources* **1995**, *54*, 522–524.
- [3] A. K. Padhi, K. S. Nanjundaswamy, C. Maquelier, S. Okada, J. B. Goodenough, *J. Electrochem. Soc.* **1997**, *144*, 1609–1613.
- [4] A. Yamada, S. C. Chung, K. Hinokuma, *J. Electrochem. Soc.* **2001**, *148*, A224–A229.
- [5] S. Islam, M. H. Alfaruqi, D. Y. Putro, V. Mathew, S. Kim, J. Jo, S. Kim, Y.-K. Sun, K. Kim, J. Kim, *ChemSusChem* **2018**, *11*, 2239–2247.
- [6] B. Venkata Rami Reddy, R. Ravikumar, C. Nithya, S. Gopukumar, *J. Mater. Chem. A* **2015**, *3*, 18059–18063.
- [7] E. Azaceta, L. Lutz, A. Grimaud, J. M. Vicent-Luna, S. Hamad, L. Yate, G. Cabañero, H.-J. Grande, J. A. Anta, J.-M. Tarascon, R. Tena-Zaera, *ChemSusChem* **2017**, *10*, 1616–1623.
- [8] J. Zhao, L. Zhao, N. Dimov, S. Okada, T. Nishida, *J. Electrochem. Soc.* **2013**, *160*, A3077–A3081.
- [9] J. Billaud, R. J. Clément, A. R. Armstrong, J. Canales-Vázquez, P. Rozier, C. P. Grey, P. G. Bruce, *J. Am. Chem. Soc.* **2014**, *136*, 17243–17248.
- [10] B. Mortemard de Boisse, D. Carlier, M. Guignard, C. Delmas, *J. Electrochem. Soc.* **2013**, *160*, A569–A574.
- [11] A. Caballero, L. Hernán, J. Morales, L. Sánchez, J. Santos Peña, M. A. G. Aranda, *J. Mater. Chem.* **2002**, *12*, 1142–1147.
- [12] P. F. Wang, H. Xin, T. T. Zuo, Q. Li, X. Yang, Y. X. Yin, X. Gao, X. Yu, Y. G. Guo, *Angew. Chem. Int. Ed.* **2018**, *57*, 8178–8183; *Angew. Chem.* **2018**, *130*, 8310–8315.
- [13] S.-M. Oh, S.-T. Myung, J. Hassoun, B. Scrosati, Y.-K. Sun, *Electrochem. Commun.* **2012**, *22*, 149–152.
- [14] T. Boyadzhieva, V. Koleva, E. Zhecheva, D. Ntihtanova, L. Mithaylov, R. Stoyanova, *RSC Adv.* **2015**, *5*, 87694–87705.
- [15] Y. Kee, N. Dimov, A. Staykov, S. Okada, *Mater. Chem. Phys.* **2016**, *171*, 45–49.
- [16] P. Barpanda, G. Liu, C. D. Ling, M. Tamaru, M. Avdeev, S.-C. Chung, Y. Yamada, A. Yamada, *Chem. Mater.* **2013**, *25*, 3480–3487.
- [17] P. Barpanda, T. Ye, M. Avdeev, S.-C. Chung, A. Yamada, *J. Mater. Chem. A* **2013**, *1*, 4194–4197.
- [18] Y. Kee, N. Dimov, A. Staikov, P. Barpanda, Y.-C. Lu, K. Minami, S. Okada, *RSC Adv.* **2015**, *5*, 64991–64996.
- [19] Y. Noguchi, E. Kobayashi, L. S. Plashnitsa, S. Okada, J.-I. Yamaki, *Electrochim. Acta* **2013**, *101*, 59–65.
- [20] J.-Z. Guo, X.-L. Wu, F. Wan, J. Wang, X.-H. Zhang, R.-S. Wang, *Chem. Eur. J.* **2015**, *21*, 17371–17378.
- [21] W. Chen, X. Zhang, L. Mi, C. Liu, J. Zhang, S. Cui, X. Feng, Y. Cao, C. Shen, *Adv. Mater.* **2019**, *31*, 1806664.
- [22] Y. Liu, Y. Fang, Z. Zhao, C. Yuan, X. W. Lou, *Adv. Energy Mater.* **2019**, *9*, 1970026.
- [23] A. Dianat, N. Seriani, M. Bobeth, G. Cuniberti, *J. Mater. Chem. A* **2013**, *1*, 9273–9280.
- [24] M. J. Aragón, P. Lavela, R. Alcántara, J. L. Tirado, *Electrochim. Acta* **2015**, *180*, 824–830.
- [25] N. V. Kosova, V. R. Podugolnikov, E. T. Devyatkina, A. B. Slobodyuk, *Mater. Res. Bull.* **2014**, *60*, 849–857.
- [26] K. Chihara, A. Kitajou, I. D. Gocheva, S. Okada, J.-I. Yamaki, *J. Power Sources* **2013**, *227*, 80–85.
- [27] N. N. Barmnik, K. Nikolowski, C. Baetz, K. G. Bramnik, H. Ehrenberg, *Chem. Mater.* **2007**, *19*, 908–915.
- [28] C. Delmas, C. Fouassier, P. Hagenmuller, J. L. Tirado, *Physica B+C* **1980**, *99*, 81–85.
- [29] A. Mendiboure, C. Delmas, P. Hagenmuller, *J. Solid State Chem.* **1985**, *57*, 323–331.
- [30] D. Yuan, X. Liang, L. Wu, Y. Cao, X. Ai, J. Feng, H. Yang, *Adv. Mater.* **2014**, *26*, 6301–6306.
- [31] F. Aguesse, J.-M. Lopez del Amo, L. Otaegui, E. Goikolea, T. Rojo, G. Singh, *J. Power Sources* **2016**, *336*, 186–195.
- [32] L. Zheng, M. N. Obrovac, *J. Electrochem. Soc.* **2016**, *163*, A2362–A2367.
- [33] R. D. Shannon, *Acta Crystalogr.* **1976**, *A32*, 751–767.
- [34] E. M. Seibel, J. H. Roudebush, H. Wu, Q. Huang, M. N. Ali, H. Ji, R. J. Cava, *Inorg. Chem.* **2013**, *52*, 13605–13611.
- [35] J. Ma, S.-H. Bo, L. Wu, Y. Zhu, C. P. Grey, P. G. Khalifah, *Chem. Mater.* **2015**, *27*, 2387–2399.
- [36] D. Kriegner, C. Panse, B. Mandl, K. A. Dick, M. Keplinger, H. M. Persson, P. Caroff, D. Ercolani, L. Sorba, F. Bechstedt, J. Stangl, G. Bauer, *Nano Lett.* **2011**, *11*, 1483–1489.
- [37] C. Frayret, E. I. Izgorodina, D. R. MacFarlane, A. Villeguzanne, A.-L. Barrès, O. Politano, D. Rebeix, P. Poizot, *Phys. Chem. Chem. Phys.* **2012**, *14*, 11398–11412.
- [38] J. M. Crowley, J. Tahir-Kheli, W. A. Goddard III, *J. Phys. Chem. Lett.* **2016**, *7*, 1198–1203.
- [39] Y. Lei, X. Li, L. Liu, G. Ceder, *Chem. Mater.* **2014**, *26*, 5288–5296.
- [40] Y. Kee, N. Dimov, A. Staykov, S. Okada, *Mater. Lett.* **2016**, *183*, 187–190.
- [41] B. M. De Boisse, M. Reynaud, J. Ma, J. Kikkawa, S.-I. Nishimura, M. Casas-Cabanas, C. Delmas, M. Okubo, A. Yamada, *Nat. Commun.* **2019**, *10*, 2185.
- [42] J. W. Somerville, A. Sobkowiak, N. Tapia-Ruiz, J. Billaud, J. G. Lozano, R. A. House, L. C. Gallingo, T. Ericsson, L. Häggström, M. R. Roberts, U. Maitra, P. G. Bruce, *Energy Environ. Sci.* **2019**, *12*, 2223–2232.
- [43] A. Saracibar, J. Carrasco, D. Saurel, M. Galceran, B. Acebedo, H. Anne, M. Lepoittevin, T. Rojo, M. Casas Cabanas, *Phys. Chem. Chem. Phys.* **2016**, *18*, 13045–13051.
- [44] A. Vasileiadis, M. Wagemaker, *Chem. Mater.* **2017**, *29*, 1076–1088.
- [45] R. Tripathi, S. M. Wood, M. S. Islam, L. F. Nazar, *Energy Environ. Sci.* **2013**, *6*, 2257–2264.
- [46] J. M. Clark, P. Barpanda, A. Yamada, M. S. Islam, *J. Mater. Chem. A* **2014**, *2*, 11807–11812.
- [47] G. Kresse, J. Furthmüller, *Phys. Rev. B* **1996**, *54*, 11169–11186.
- [48] G. Kresse, D. Joubert, *Phys. Rev. B* **1999**, *59*, 1758–1775.

Manuscript received: October 30, 2019

Revised manuscript received: November 27, 2019

Accepted manuscript online: December 20, 2019

Version of record online: January 14, 2020